scientific reports

Check for updates

OPEN

Preservation of masseter muscle until the end stage in the SOD1G93A mouse model for ALS

Sou Kawata[1], Soju Seki[1]✉, Akira Nishiura[1], Yoshihiro Kitaoka[3], Kanako Iwamori[2], So-ichiro Fukada[2], Mikihiko Kogo[1] & Susumu Tanaka[1]

Amyotrophic lateral sclerosis (ALS) progressively impairs motor neurons, leading to muscle weakness and loss of voluntary muscle control. This study compared the effects of SOD1 mutation on masticatory and limb muscles from disease onset to death in ALS model mice. Notably, limb muscles begin to atrophy soon after ALS-like phenotype appear, whereas masticatory muscles maintain their volume and function in later stages. Our analysis showed that, unlike limb muscles, masticatory muscles retain their normal structure and cell makeup throughout most of the disease course. We found an increase in the number of muscle satellite cells (SCs), which are essential for muscle repair, in masticatory muscles. In addition, we observed no reduction in the number of muscle nuclei and no muscle fibre-type switching in masticatory muscles. This indicates that masticatory muscles have a higher resistance to ALS-related damage than limb muscles, likely because of differences in cell composition and repair mechanisms. Understanding why masticatory muscles are less affected by ALS could lead to the development of new treatments. This study highlights the importance of studying different muscle groups in ALS to clarify disease aetiology and mechanisms.

Keywords Amyotrophic lateral sclerosis, Masseter muscles, Gastrocnemius muscle, Satellite cells, Voluntary muscle control

Amyotrophic lateral sclerosis (ALS) is a neurodegenerative disease that progressively impairs the motor neurons responsible for voluntary muscle control. The incidence rate of ALS is 2.16 per 100,000 individuals in Western countries, with approximately half of the patients dying within three years[1]. ALS typically starts with weakening limb muscles, leading to muscle wasting and paralysis caused by neuronal degeneration. People with ALS often lose body weight rapidly owing to muscle loss and increased metabolism[2]. In the later stages, weakened diaphragmatic muscles are a common cause of death. ALS also causes bulbar palsy symptoms, such as dysphagia and speech disorders, along with tongue atrophy and diminished throat reflexes[3]. These symptoms are included in the ALS Functional Rating Scale-Revised (ALSFRS-R), which evaluates the severity of ALS[4].

The specific cause of ALS, and particularly why it targets motor neurons, remains unclear. Current ALS treatments, such as riluzole and edaravone, only slightly prolong life expectancy, highlighting the critical need for more effective therapies[5]. Recent studies have explored the involvement of sensory neurons, which is a previously overlooked area, in ALS, and the possibility of targeting sensory neurons to treat ALS is being explored[6–9].

Although swallowing difficulties in patients with ALS are known, the full extent of changes in masticatory function is less understood. Previous studies with neonatal SOD1G93A mice (mSOD1) have reported irregular activity in trigeminal motor neurons (MoV) and mesencephalic trigeminal neurons (MesV), which are important for mastication[6,10,11], and that the MoV subsequently undergoes degeneration, similar to other motor neurons[12–15]. However, detailed documentation of changes in the peripheral masticatory muscles of these mice over time is lacking. In ALS, although many muscles weaken and become paralysed, some muscles, such as those controlling eye movements and the external sphincter muscles, remain relatively unaffected. This retention of function in certain muscles enables patients with ALS to maintain eye movement and bladder and bowel control until the later stages of the disease, allowing them to use eye-tracking devices for computer-based communication[16].

[1]Department of Oral and Maxillofacial Surgery, Graduate School of Dentistry, Osaka University, 1-8 Yamadaoka, Suita, Osaka 565-0871, Japan. [2]Laboratory of Stem Cell Regeneration and Adaptation, Graduate School of Pharmaceutical Sciences, Osaka University, 1-6 Yamadaoka, Suita, Osaka 565-0871, Japan. [3]University California, Los Angeles, School of Dentistry, Section of Biosystems and Function, Laboratory of Neuropharmacology, 714 Tiverton Los Angeles, CA 90095, United States. ✉email: seki.soju.dent@osaka-u.ac.jp

Recent studies have highlighted the significant role of skeletal muscle in ALS, positioning it as a potential therapeutic target. The "dying back" theory of ALS involves not only unilateral disease transmission from neurons to muscle, but also from muscle to neurons. In this theory, muscle initiates, or at least contributes to, a series of pathological events that promote the distal onset of motor neuron degeneration[17,18]. These muscles can regenerate and adapt, but require protein production and increased muscle fibre nuclei for repair and growth[19,20]. Satellite cells (SCs), which are the stem cells within skeletal muscles, are crucial to this process[21–25]. The SCs, although normally inactive, become activated in response to injury or mechanical loading. Pax7, a well-known SC marker, is expressed in the early phase, while MyoD is expressed in the active phase[26].

Skeletal muscles are generally categorised into two types based on the myosin heavy chain (MyHC): slow-twitch (MyHC-I) and fast-twitch (MyHC-II) fibres. Slow-twitch fibres, which resist fatigue, are used for prolonged activities, whereas fast-twitch fibres, which rapidly fatigue, can execute high-intensity activities. The ratio of these fibre types can vary under different conditions, thereby influencing muscle properties[27]. Various diseases affect these muscle fibres differently. In ALS, muscle wasting typically begins in fast-twitch fibres in both patients and mouse models. As the disease progresses, the metabolic state of the fibres shifts from glycolytic to oxidative metabolism, specifically, a switch from MyHCIIb to MyHCIIx, and eventually to MyHCIIa[28,29].

In our study, we analysed both behavioural and physiological changes in masticatory function and muscle volume in ALS using mSOD1 from birth to death. We compared the masticatory muscle tissue with limb muscle tissue before and after the onset of symptoms via fluorescent immunostaining. This approach enabled us to observe changes in the volume, function, and microscopic structure of the muscle fibres in the masticatory muscles of mice. Our findings offer new insights into the relatively unexplored aspects of masticatory function in patients with ALS.

Results

Masticatory function in mSOD1 declines less with time than limb motor function

We observed the behaviour of mSOD1 and wild-type mice (WT) from 4 to 16 weeks of age to assess masticatory and limb motor functions. In both mSOD1 and WT groups, there was a downward trend in feeding time starting at 14 weeks and in food consumption starting at 12 weeks, yet no significant differences were found across all ages (Fig. 1a, b). With regard to motor function, the mSOD1 group showed a decline in treadmill running distance after 10 weeks, which became significant after 14 weeks. The WT group maintained an increasing trend in running distance at all ages, reaching nearly full completion. A notable decrease in running distance was observed in the mSOD1 group from 16 weeks ($F(1, 117) = 9.37$, $p < 0.001$; 12 week: mSOD1, 936 ± 87.01 m, WT, 1060.92 ± 45.98 m, $p = 0.20$; 14 week: mSOD1, 734.46 ± 150.98 m, WT, 964.46 ± 71.49 m, $p = 0.16$, 16 week: mSOD1, 290 ± 119.59 m, WT, 1061.15 ± 37.73 m, $p = 0.003$, repeated-measures ANOVA and Tukey–Kramer post-hoc comparison, Fig. 1c). The grip strength in the mSOD1 group started to decrease after 10 weeks, similar to the treadmill running performance. The WT group exhibited an increasing trend in grip strength from 8 weeks onwards. A significant reduction in grip strength was noted in the mSOD1 group starting at 14 weeks ($F(1, 133) = 10.02$, $p < 0.001$; 12 week: mSOD1, 165.39 ± 15.51 g, WT, 185.83 ± 10.88 g, $p = 0.30$, 14 week: mSOD1, 152.12 ± 15.96 g, WT, 192.93 ± 8.66 g, $p = 0.042$, 16 week: mSOD1, 132.47 ± 25.15 g, WT, 211.98 ± 17.44 g, $p = 0.017$, repeated-measures ANOVA and Tukey–Kramer post-hoc comparison, Fig. 1d). The body weight in the mSOD1 group initially increased until 10 weeks but started to decline after 12 weeks, whereas the WT group showed consistent weight gain throughout the observation period. However, no significant differences in body weight were observed between groups (Fig. 1e). Survival curves from 6 to 20 weeks for the mSOD1 and WT groups are shown (Week 17: mSOD1, 0.73; WT, 1.00; Week 18: mSOD1, 0.55; WT, 1.00; Week 19: mSOD1, 0.27; WT, 1.00; Week 20: mSOD1, 0.18; WT, 1.00).

Masseter muscle volume in mSOD1 mice shows less volume loss over time than limb skeletal muscle volume

We assessed the temporal changes in muscle volume related to feeding and limb motor function (Fig. 2a). Micro-CT allows for a more accurate assessment of changes in muscle volume compared to methods that evaluate muscle cross-sectional area. Additionally, changes in muscle volume over time can be observed in mice using hindlimb micro-CT images without contrast[30]. In the masseter muscle, an upward trend was observed until week 14. The WT group consistently showed increased muscle volume across all ages, paralleling body weight growth. However, there were no significant differences between groups at any age ($F(1, 145) = 3.35$, $p = 0.069$, 12 weeks: mSOD1, 35.93 ± 2.43 mm^3, WT, 31.47 ± 2.61 mm^3, $p = 0.23$, 14 weeks: mSOD1, 37.66 ± 1.79 mm^3, WT, 35.77 ± 2.29 mm^3, $p = 0.52$, 16 weeks: mSOD1, 34.99 ± 3.29 mm^3, WT, 37.42 ± 2.45 mm^3, $p = 0.56$; repeated-measures ANOVA and Tukey–Kramer post-hoc comparison, Fig. 2b). Regarding forelimb muscles, the mSOD1 group displayed a downward trend from 10 weeks onwards, whereas the WT group showed an increase throughout the study period. There were no significant differences between groups with regard to changes in forelimb muscle volume ($F(1, 144) = 0.60$, $p = 0.44$, 12 weeks: mSOD1, 76.27 ± 4.96 mm^3, WT, 71.14 ± 5.73 mm^3, $p = 0.50$, 14 weeks: mSOD1, 72.95 ± 4.14 mm^3, WT, 76.76 ± 4.63 mm^3, $p = 0.55$, 16 weeks: mSOD1, 70.71 ± 4.51 mm^3, WT, 84.56 ± 7.65 mm^3, $p = 0.15$; repeated-measures ANOVA and Tukey–Kramer post-hoc comparison, Fig. 2c). In the hind limb muscles, a decrease in volume began at 8 weeks in the mSOD1 group, whereas the WT group experienced a volume increase at all ages. A significant volume reduction was observed in the mSOD1 group at 16 weeks ($F(1, 143) = 5.13$, $p < 0.001$, 12 weeks: mSOD1, 178.87 ± 9.43 mm^3, WT, 203.7 ± 20.18 mm^3, $p = 0.25$, 14 weeks: mSOD1, 175.95 ± 10.31 mm^3, WT, 222.15 ± 20.93 mm^3, $p = 0.056$, 16 weeks: mSOD1, 151.01 ± 15.44 mm^3, WT, 259.24 ± 18.51 mm^3, $p < 0.001$; repeated-measures ANOVA and Tukey–Kramer post-hoc comparison, Fig. 2d).

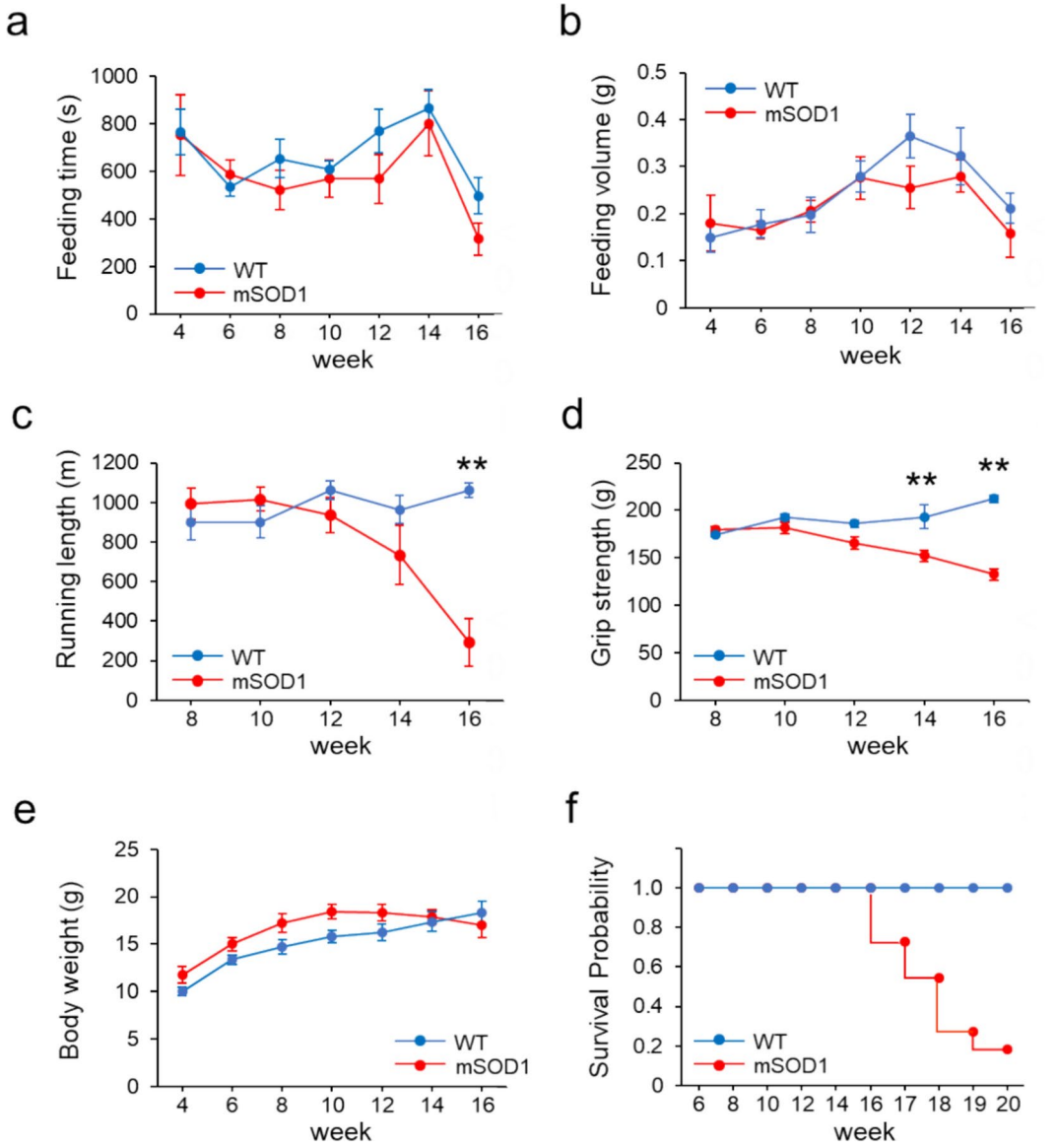

Fig. 1. (**a**), (**b**) Feeding duration and total food consumption from 4 to 16 weeks. No notable differences in feeding time or amount of food consumed were observed between the groups. (**c**) Distance covered on a treadmill from 4 to 16 weeks. The mSOD1 group showed a significant decrease in running distance beginning at 16 weeks [mSOD1 (n = 11), WT (n = 10), analyzed using repeated-measures ANOVA and Turkey-Kramer post hoc comparison, $p = 0.003$, $^{**}p < 0.01$]. (**d**) Limb grip strength from 4 to 16 weeks. The mSOD1 group experienced a marked reduction in grip strength starting at 14 weeks [mSOD1 (n = 11), WT (n = 10), analyzed using repeated-measures ANOVA and Turkey-Kramer post hoc comparison, p = 0.002, $^{**}p < 0.01$]. (**e**) Body weight changes from 4 to 16 weeks. A downward trend in body weight was noted in the mSOD1 group starting at 10 weeks, although this change was not statistically significant. (**f**) In the survival curve from 6 to 20 weeks, mSOD1 group survived about half at 18 weeks [mSOD1 (n = 11), WT (n = 10)].

The decrease in masseter wet weight in mSOD1 mice at the late stage of ALS is lower than the decrease in gastrocnemius wet weight

To evaluate skeletal muscle health, we measured the wet weights of the masseter and gastrocnemius muscles in mSOD1 and WT at 8 and 16 weeks. At 8 weeks, there was no significant difference in the wet weights of either muscle between the mSOD1 and WT groups (masseter: 8 weeks: mSOD1, 0.1000 ± 0.0033 g, WT, 0.0892 ± 0.0040 g, $p = 0.050$; gastrocnemius: 8 weeks: mSOD1, 0.1016 ± 0.0122 g, WT, 0.1271 ± 0.0046 g, $p = 0.067$, assessed using student-*t* test, Fig. 3a and b). By 16 weeks, a notable decrease in wet weight was observed in the gastrocnemius muscle in the mSOD1 group, while no significant difference was observed in the wet weight of the masseter muscle (masseter: 16 weeks: mSOD1, 0.0770 ± 0.0042 g, WT, 0.0820 ± 0.0043 g, $p = 0.35$; gastrocnemius: 16 weeks: mSOD1, 0.0680 ± 0.0064 g, WT, 0.1310 ± 0.0098 g, $p < 0.001$, analysed using student-*t* test, Fig. 3a and b).

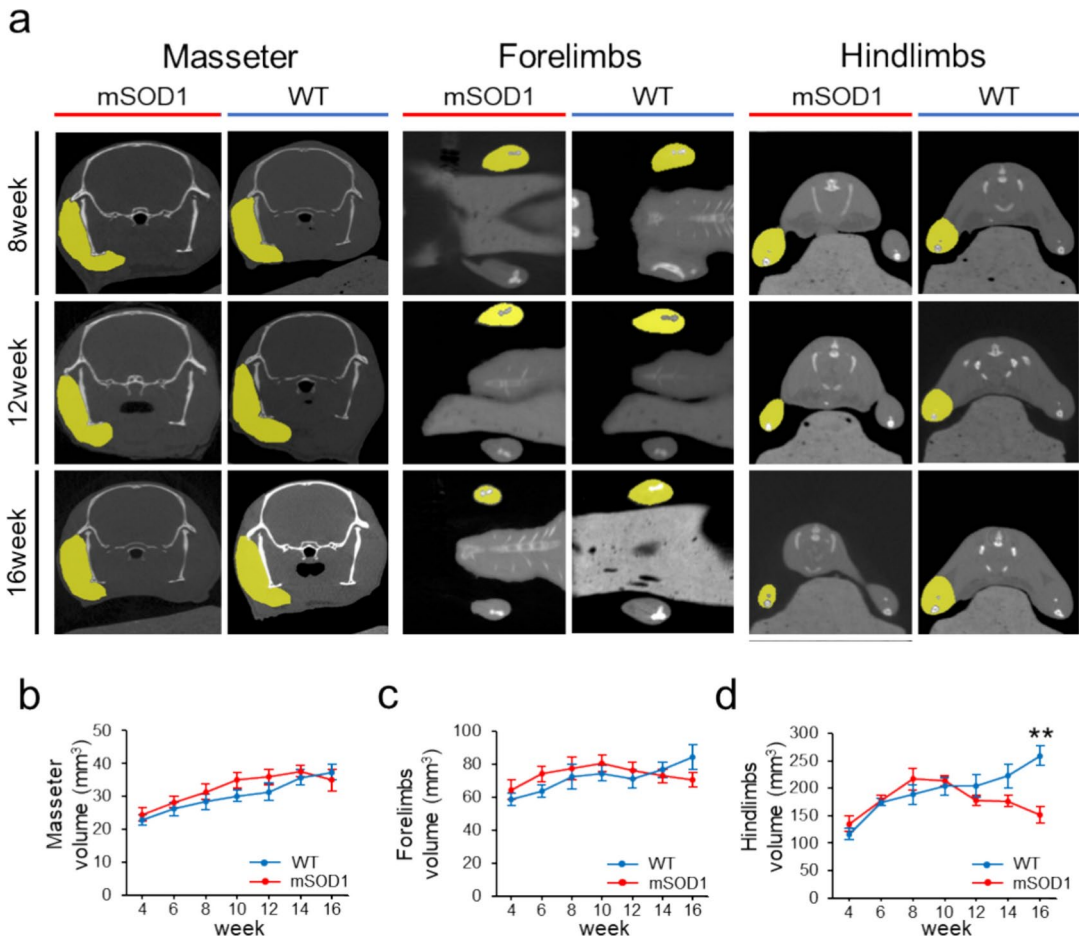

Fig. 2. Changes in Muscle Volume of the Masseter and Limb Skeletal Muscles (**a**) Micro-CT images (outlined in yellow) displaying the masseter, forelimb, and hindlimb muscles in both mSOD1 and WT groups at 8, 12, and 16 weeks. (**b**) Analysis of masseter muscle volume from 4 to 16 weeks showed no notable differences between groups. (**c**) Forelimb muscle volume changes from 4 to 16 weeks showed a downward trend in the mSOD1 group starting at 10 weeks, although not statistically significant. (**d**) Hindlimb muscle volume changes from 4 to 16 weeks demonstrated a decline in the mSOD1 group starting at 8 weeks, with a significant reduction at 16 weeks [mSOD1 (n = 11), WT (n = 10), analysed by repeated-measures ANOVA and Turkey–Kramer post-hoc comparison, $^{*}p < 0.001$, $^{**}p < 0.01$].

The number and cross-sectional area of myofibers in the masseter muscle are not reduced in mSOD1 at the late stage of ALS

We investigated the histological changes in the masseter and gastrocnemius muscles of mSOD1 and WT mice at 8 and 16 weeks of age (Fig. 4a). Our study found no significant difference in the total number of muscle fibres in either muscle type between the mSOD1 and WT groups. In particular, for the masseter muscle at 8 weeks, the mSOD1 group showed an average of 1433.8 ± 267.51 fibres, and the WT group showed an average of 1157.20 ± 230.30 fibres ($p = 0.46$). At 16 weeks, these numbers were 1497.4 ± 396.53 and 1395.2 ± 310.22 in the mSOD1 and WT groups, respectively ($p = 0.84$). In the gastrocnemius muscle, the counts were 2122.8 ± 489.08 and 2597.2 ± 593.91 in the mSOD1 and WT group at 8 weeks ($p = 0.54$) and 1796.8 ± 374.41 and 2492.6 ± 210.56 in the mSOD1 and WT groups at 16 weeks, respectively ($p = 0.14$) (Figs. 4b and c).

Regarding the fibre cross-sectional area in the masseter muscle, both groups showed no significant difference at 8 weeks (mSOD1: 1214.80 ± 105.74 μm^2, WT: 1455.40 ± 175.69 μm^2, $p = 0.27$) and 16 weeks (mSOD1: 1700.60 ± 189.47 μm^2, WT: 1528.20 ± 85.87 μm^2, $p = 0.43$) (Fig. 4d). However, concerning the gastrocnemius muscle, the mSOD1 group displayed notably smaller fibre areas than the WT group at both 8 weeks (mSOD1: 1361.60 ± 26.08 μm^2, WT: 1567.60 ± 56.12 μm^2, $p = 0.010$) and 16 weeks (mSOD1: 1200.80 ± 80.18 μm^2, WT: 1671.20 ± 56.12 μm^2, $p = 0.023$) (Fig. 4e).

Masseter muscles showed no change in the percentage of MyHC fibers in mSOD1 at the late stage of ALS

Skeletal muscle fibres can be categorised into four types based on the Myosin Heavy Chain (MyHC): MyHC-I (slow-twitch fibres) and three types of MyHC-II (fast-twitch fibres), namely MyHC-IIa, MyHC-IIb, and MyHC-IIx[31]. For the remaining fibers other than MyHC-I, IIa, and IIb, most are considered to be MyHC-IIx. In this

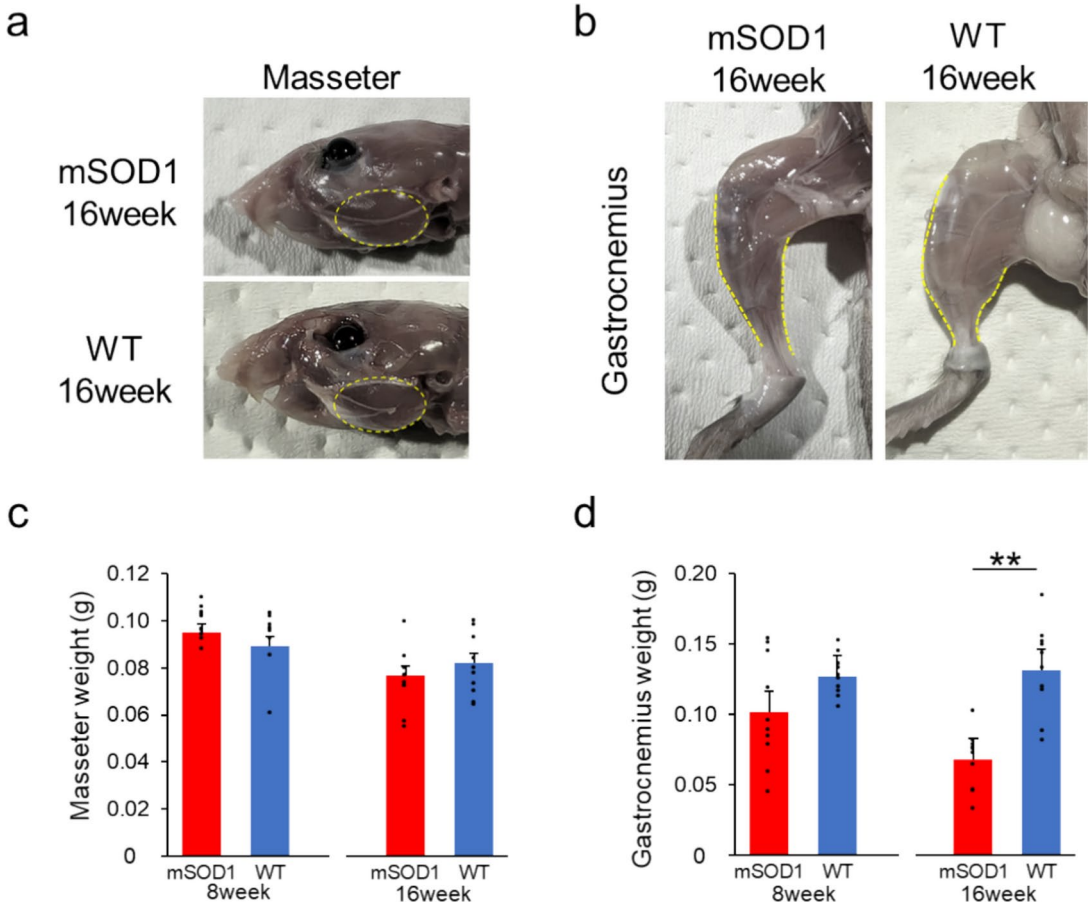

Fig. 3. Muscle Weight Analysis (a) The masseter muscle in mSOD1 and WT groups at 16 weeks of age, respectively. (**b**) The gastrocnemius muscle in mSOD1 and WT groups at 16 weeks of age, respectively. (**c**) The wet weight of the masseter muscle in mSOD1 and WT groups at 8 and 16 weeks. There were no significant differences observed between the groups. (**d**) The wet weight of the gastrocnemius muscle in mSOD1 and WT groups at 8 and 16 weeks. At 16 weeks, the mSOD1 group had significantly lower values compared to the WT group [8 weeks (mSOD1: n = 5, WT: n = 5), 16 weeks (mSOD1: n = 5, WT: n = 5), as assessed by Student's t-test, $p < 0.01$, $^{**}p < 0.01$].

study, we analysed MyHC-I, MyHC-IIa, and MyHC-IIb (Fig. 5a). In both masseter and gastrocnemius muscles, the order of prevalence of each fibre type was MyHC-IIb > MyHC-IIa > MyHC-I, indicating a similar pattern for both muscles.

Upon further examining the masseter muscle, no significant differences were observed in the proportion of each muscle fibre type between the mSOD1 and WT groups at 8 or 16 weeks (Fig. 5b). In contrast, in the gastrocnemius muscle, although there were no notable differences in the proportions of MyHC-I and MyHC-IIa fibre types at 8 and 16 weeks, a significant difference was observed in the proportion of MyHC-IIb fibres at 16 weeks between groups. The mSOD1 group showed a significantly lower proportion of MyHC-IIb fibres (0.522 ± 0.018) than the WT group (0.694 ± 0.037, $p < 0.001$, student-*t* test, Fig. 5c).

Pax7-positive SCs are increased in masseter muscle at the late-stage mSOD1

The masseter and gastrocnemius muscles were stained with Pax7, Laminin, and DAPI for immunofluorescence analysis. This allowed us to measure the number of muscle fibre nuclei and Pax7-positive SCs (Fig. 6a). In the masseter muscle, there were no significant differences in the number of muscle fibre nuclei between the mSOD1 and WT groups at both 8 and 16 weeks (Fig. 6b). However, in the gastrocnemius muscle, although the WT group maintained consistent numbers of muscle fibre nuclei between 8 and 16 weeks, the mSOD1 group exhibited a significant decrease at 16 weeks (8 weeks: myonucleus/fibre = 2.772 ± 0.161, 16 weeks: myonucleus/fiber = 1.719 ± 0.608, $p = 0.010$, student-*t* test, Fig. 6c).

In terms of Pax7-positive SCs, the masseter muscle displayed approximately double the number observed in the gastrocnemius muscle. Within the masseter muscle, the WT group showed an increasing trend for Pax7-positive SC numbers from 8 to 16 weeks, although this was not statistically significant. Notably, in the mSOD1 group, there was a significant increase in Pax7-positive SCs at 16 weeks compared with 8 weeks (8 weeks: Pax7-positive SCs/100 fibres = 7.13 ± 3.86, 16 weeks: Pax7-positive SCs/100 fibres = 14.69 ± 5.92, $p = 0.044$, student-*t* test, Fig. 6d). For the gastrocnemius muscle, both mSOD1 and WT groups indicated an upward trend in

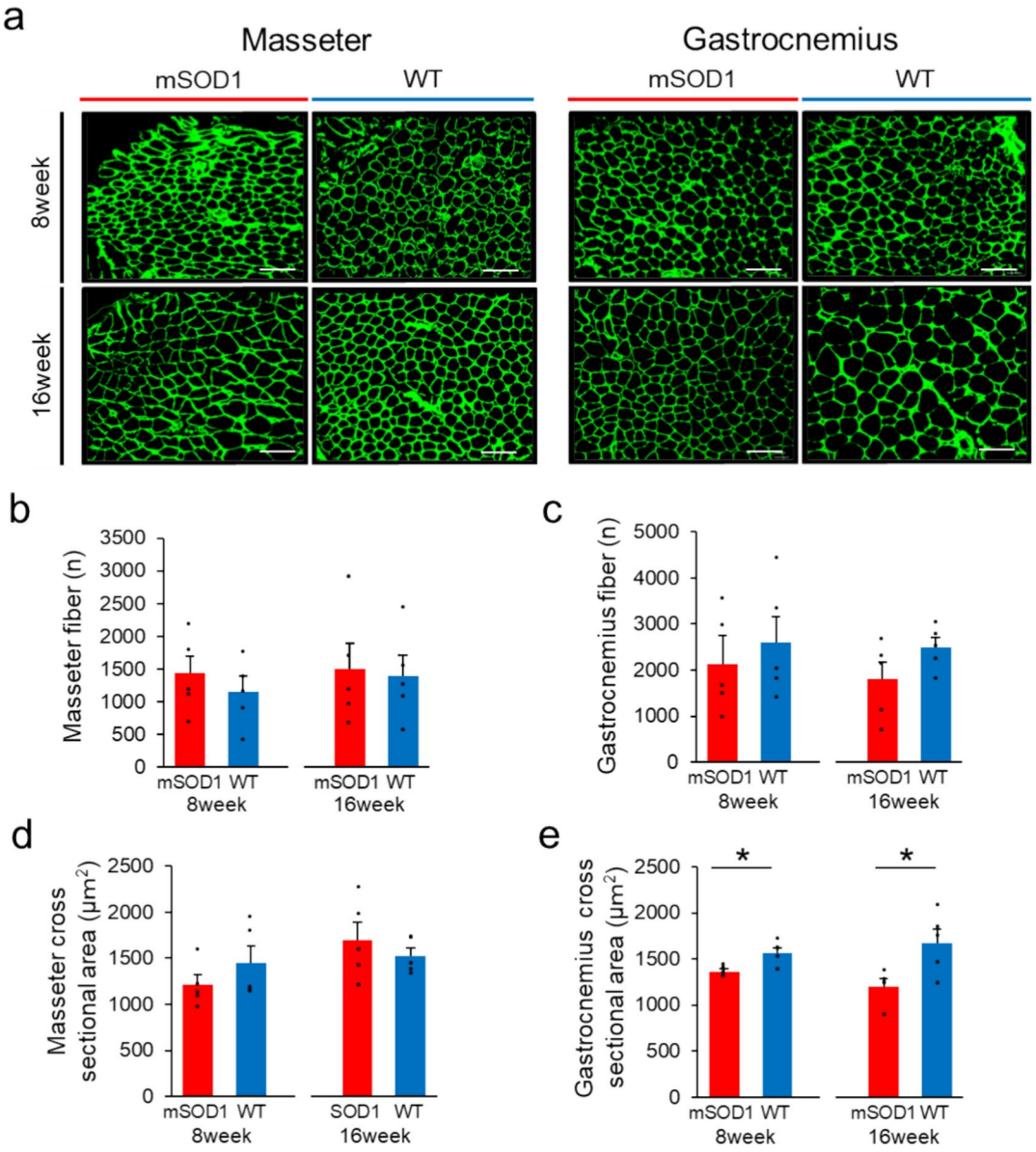

Fig. 4. Analysis of Muscle Fibre Count and Cross-Sectional Area (**a**) Fluorescent immunostaining showing Laminin (green) in the masseter and gastrocnemius muscles for both mSOD1 and WT groups at 8 and 16 weeks (scale bar: 100 μm). (**b**) Counts of muscle fibres in the masseter muscle in the mSOD1 and WT groups at 8 and 16 weeks, with no significant differences observed between the groups. (**c**) Counts of muscle fibres in the gastrocnemius muscle for mSOD1 and WT groups at 8 and 16 weeks, showing no significant differences. (**d**) Analysis of the cross-sectional area of muscle fibres in the masseter muscle in both groups at 8 and 16 weeks showed no significant differences. (**e**) Cross-sectional area of muscle fibres in the gastrocnemius muscle at 8 and 16 weeks indicated significantly smaller areas in the mSOD1 group at both time points [8 weeks (mSOD1: n = 5, WT: n = 5), 16 weeks (mSOD1: n = 5, WT: n = 5), as assessed by Student's t-test, 8 weeks: $p = 0.010$, 16 weeks: $p = 0.022$, $^{*}p < 0.05$].

Pax7-positive SC numbers over time, but these changes were not statistically significant (mSOD1: 8 weeks, Pax7-positive SCs/100 fibres = 3.26 ± 0.16, 16 weeks, Pax7-positive SCs/100 fibres = 6.59 ± 1.851, $p = 0.11$; WT: 8 weeks, Pax7-positive SCs/100 fibres = 3.45 ± 1.04, 16 weeks, Pax7-positive SCs/100 fibres = 3.86 ± 1.52, $p = 0.83$, student-*t* test, Fig. 6e).

Pax7-positive satellite cells were increased, whereas MyoD-positive satellite cells were not increased in the masseter muscle of end-stage mSOD1.

Brainstem slices, masseter, and gastrocnemius muscles were removed from three mSOD1 that survived to 18 weeks to explore the mechanism by which the masseter is preserved until the end stage. H&E staining of brainstem slices containing the MoV region, which controls masseter muscle movement, revealed numerous vacuolations in all three mSOD1 (Fig. 7a). We investigated the histological changes in the masseter and

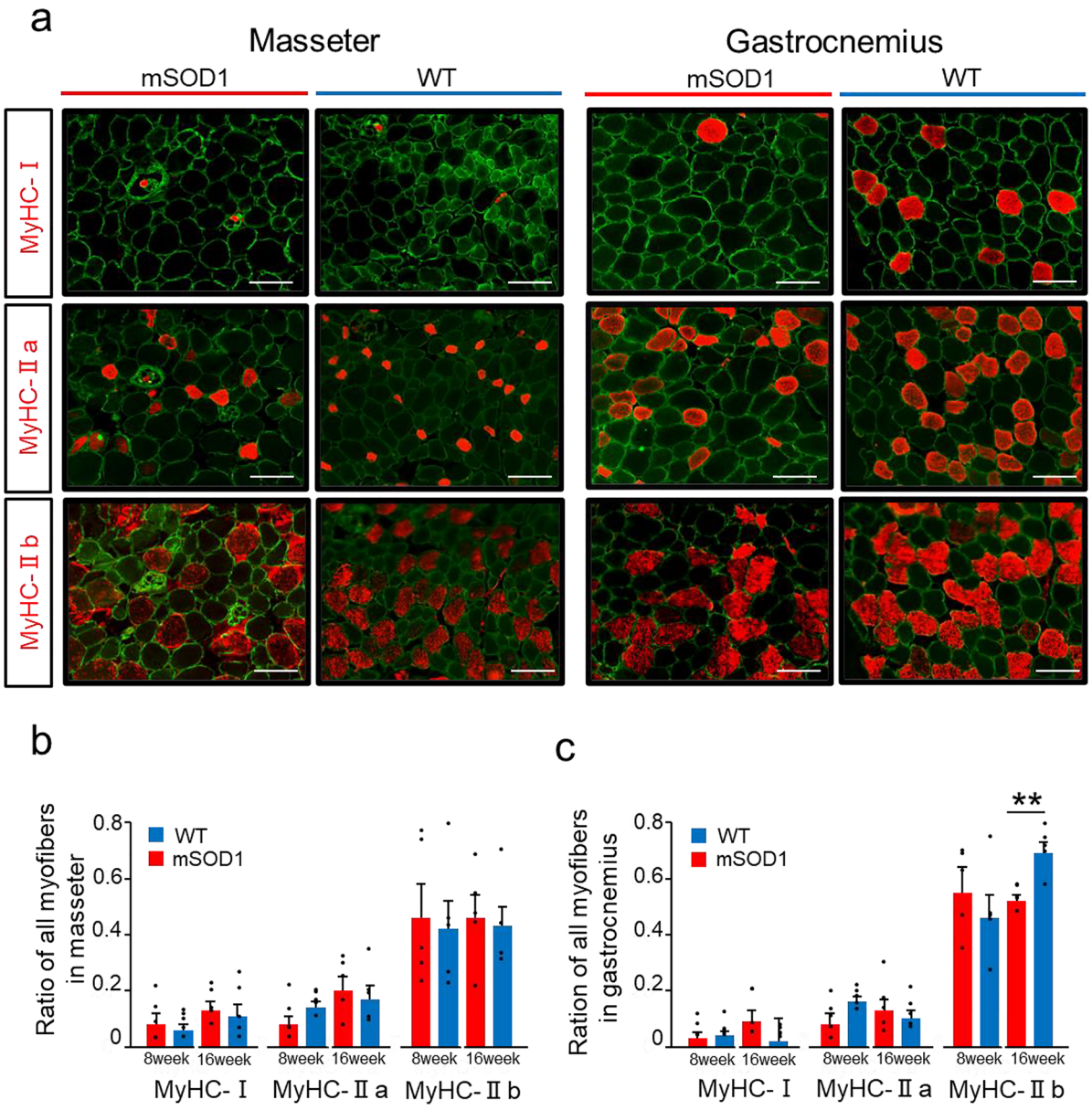

Fig. 5. Distribution of Muscle Fibre Types (**a**) Fluorescent immunostaining illustrates Laminin (green) and various MyHC types (red) in the masseter and gastrocnemius muscles in mSOD1 and WT groups at 16 weeks (scale bar: 20 µm). (**b**) The proportion of each muscle fibre type in the masseter muscle showed no significant differences between mSOD1 and WT groups at 8 and 16 weeks. (**c**) The proportion of muscle fibre types in the gastrocnemius muscle at 16 weeks, with a notably lower proportion of MyHC-IIb fibres in the mSOD1 group compared with WT [MyHC-IIb, 16 weeks (mSOD1: n = 5, WT: n = 5), as analysed using Student's t-test, $p = 0.003$, $^{**}p < 0.01$].

gastrocnemius muscles of mSOD1 and WT 18 weeks of age (Fig. 7b). Regarding the fibre cross-sectional area in the masseter muscle, both groups showed no significant difference at 18 weeks (mSOD1: 1510.67 ± 138.62 µm^2, WT: 1657.33 ± 270.22 µm^2, $p = 0.27$, Fig. 7c). However, regarding the gastrocnemius muscle, the mSOD1 group displayed notably smaller fibre areas than the WT group at 18 weeks (mSOD1: 1138.00 ± 170.53 µm^2, WT: 2188.677 ± 215.73 µm^2, $p = 0.021$, student-t test, Fig. 7d). The masseter and gastrocnemius muscles were stained with Pax7, MyoD, Laminin, and DAPI for immunofluorescence analysis. This allowed us to measure the fibre cross-sectional area in the muscle and the number of Pax7-positive SCs and MyoD-positive SCs (Fig. 7e). In the masseter in mSOD1, the number of Pax7-positive SCs was significantly increased compared to WT, but there was no difference in the number of MyoD-positive SCs (mSOD1: Pax7-positive SCs/100 fibres = 13.08 ± 1.42, WT: Pax7-positive SCs/100 fibres = 5.84 ± 1.02, $p = 0.014$, mSOD1: MyoD-positive SCs/100 fibres = 5.58 ± 1.31, WT: MyoD-positive SCs/100 fibres = 6.04 ± 0.91, $p = 0.789$, student-t test, Fig. 7f). Pax7 and MyoD-positive SCs counts in the gastrocnemius of mSOD1 were not significantly different from those in the WT (mSOD1: Pax7-positive SCs/100 fibres = 7.35 ± 1.86, WT: Pax7-positive SCs/100 fibres = 5.74 ± 1.62, $p = 0.549$, mSOD1: MyoD-

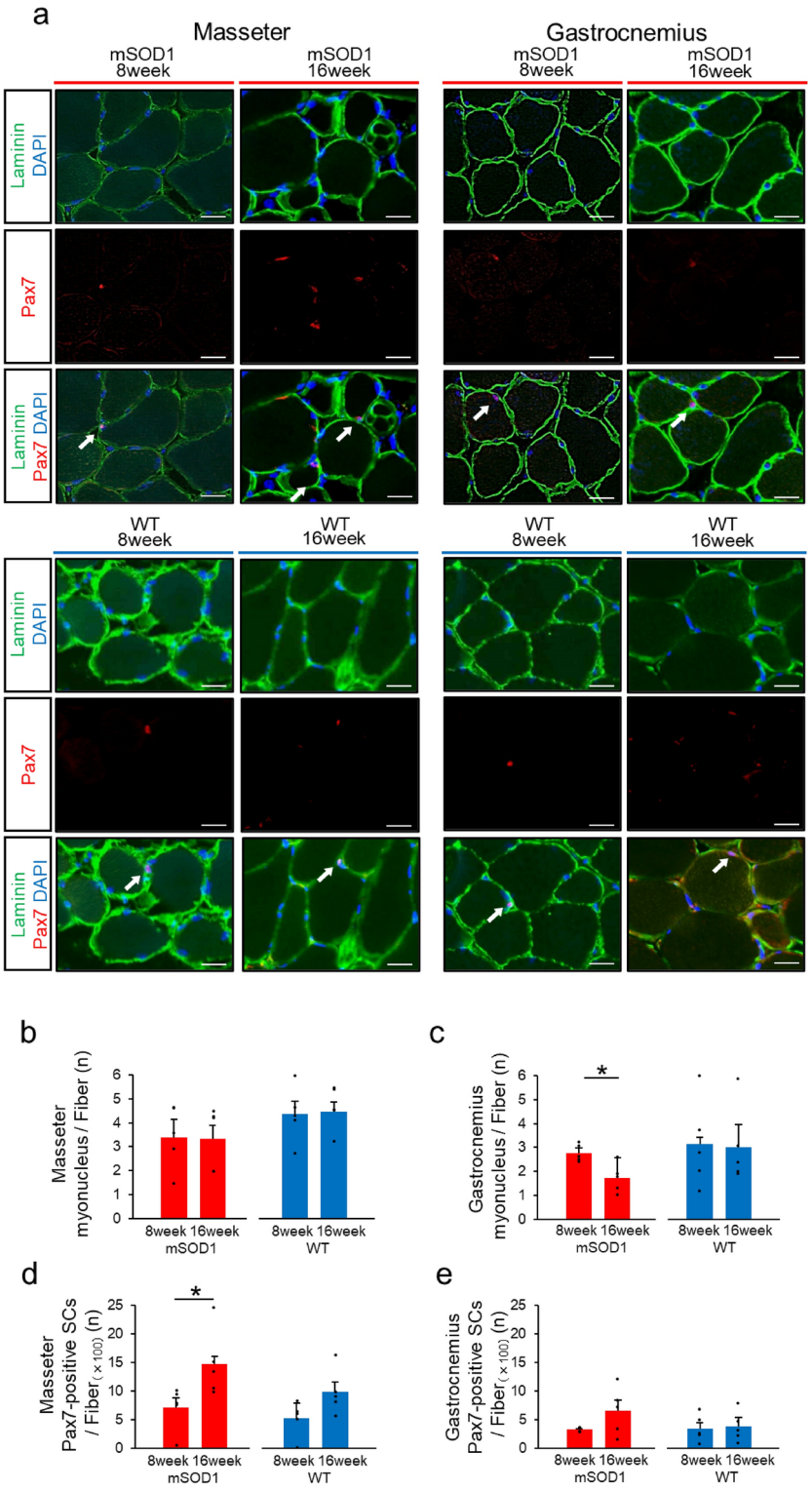

Fig. 6. Analysis of Muscle Fibre Nuclei and Satellite Cells (**a**) Immunofluorescence staining displaying Laminin (green), DAPI (blue), and Pax7 (red) in the. masseter and gastrocnemius muscles in the mSOD1 and WT group at 16 weeks (scale bar: 20 µm). Arrows point to Pax7-positive satellite cells. (**b**) Counts of nuclei per muscle fibre in the masseter muscle in mSOD1 and WT groups, showing no significant age-related differences. (**c**) In the gastrocnemius muscle in the mSOD1 group, a significant decrease was observed in the number of nuclei per muscle fibre at 16 weeks compared with 8 weeks [mSOD1 (8 weeks: n = 5, 16 weeks: n = 5), WT (8 weeks: n = 5, 16 weeks: n = 5), as assessed by Student's t-test, $p = 0.010$, $^{*}p < 0.05$). (**d**) Pax7-positive satellite cell count per 100 muscle fibres in the masseter muscle in the mSOD1 group increased significantly at 16 weeks compared with 8 weeks [mSOD1 (8 weeks: n = 5, 16 weeks: n = 5), WT (8 weeks: n = 5, 16 weeks: n = 5), as assessed by Student's t-test, $p = 0.040$, $^{*}p < 0.05$). (**e**) The counts of Pax7-positive satellite cells per 100 muscle fibres in the gastrocnemius muscle in mSOD1 and WT groups showed no significant age-related differences.

positive SCs/100 fibres = 3.49 ± 1.05, WT: MyoD-positive SCs/100 fibres = 4.43 ± 1.25, $p = 0.789$, student-t test, Fig. 7g).

Discussion

Our study focused on the masseter muscle, a crucial masticatory muscle in mSOD1. We observed that this muscle did not exhibit a reduction in volume until the late stages after symptom onset, thereby effectively preserving masticatory function. Histological analysis conducted before and after symptom onset showed that the cross-sectional area of the masseter muscle fibres was maintained. In addition, there was an increase in the number of SCs, and the muscle fibre nuclei were preserved. These observations lead us to suggest that the masseter muscles in mSOD1 are resistant to muscle atrophy. Consequently, masticatory function in these mice may remain intact until the end stage of the disease.

Patients with ALS commonly experience rapid weight loss, often because of decreased muscle mass, dysphagia, and increased metabolism[2]. mSOD1, a mouse model of ALS used in our study, survived 105–135 days[13] and showed slow weight loss after onset, with no significant weight loss in the later stages. However, the pattern of weight loss during disease progression varied between studies[32,33].

In SOD1G93A mice, trigeminal motoneurons, which are central to masticatory movements, have been reported to undergo degeneration as well as spinal motoneurons[6,10–15]. However no decrease in feeding time or food intake was observed after the onset of the disease with respect to feeding function, which confirms the results of Kitaoka et al.[6]. Micro-CT imaging showed that the masseter muscle volume in mSOD1 was preserved even after the onset of ALS-like symptoms, and the muscle wet weight did not decrease until the late stage of the disease. Since it is generally believed that patients with ALS lose masticatory strength during the oral phase of swallowing, the preservation of masticatory muscles in mSOD1 until the end of the disease is an important observation. To date, no study has investigated the cause of this phenomenon[34].

Eye movements in mSOD1 are not impaired until the end of life, unlike in patients with ALS. This is because the motoneurons innervating the external eye muscles are not impaired[11,35]. In SOD1G93A mice, there is a vulnerability gradient among motor neurons, with less excitable motor units being affected earlier[13]. Denervation differs between slow and fast-twitch muscles, with fast-twitch fatigable motoneurons degenerating more readily than fast-twitch fatigue-resistant motoneurons. This results in less denervation in the relatively resistant slow-twitch soleus muscle compared to the more vulnerable fast-twitch tibialis anterior and gastrocnemius muscles[13,18]. However, the masseter muscle in mSOD1 was preserved until the end stage of the disease despite the impairment of the center of the masticatory movement, suggesting that the masseter muscle may have a resistance mechanism against atrophy. Therefore, in this study, we compared the masseter and gastrocnemius muscles of mSOD1, which are considered fast-twitch muscles, from pre-onset to end-stage[32,36].

In a previous study, a decrease in hindlimb muscle mass was observed at 8 weeks of age, before the onset of symptoms[37]. In our study, a decrease in hindlimb muscle mass was observed from 8 weeks of age, supporting this trend. For the forelimbs, a trend toward decreased muscle mass was observed from 10 weeks of age, but the impairment associated with symptom progression was less severe than in the hindlimbs. A significant decrease in grip strength was observed earlier than the decline in treadmill running ability, and these findings were consistent with changes in muscle mass. The significant decline in grip strength, observed earlier than the decline in treadmill running ability, may be due to the grip strength test's dependence on fast-twitch muscles[38]. Since ALS is known to target these muscles for atrophy[39], our findings suggest an early-stage dysfunction of fast-twitch muscle fibres.

In this study, the muscle wet weight of the gastrocnemius muscle in late-stage mSOD1 was significantly reduced compared to wild-type mice, while the muscle wet weight of the masseter muscle showed no reduction. In the late phase, there was no reduction in the number of myofibres in either muscle. However, there was a decrease in myofiber cross-sectional area in the gastrocnemius muscle, similar to the previous study, but no decrease in myofiber cross-sectional area in the masseter muscle[37]. This trend was also observed in the end-stage mSOD1, suggesting that the loss of muscle mass in the gastrocnemius muscle was due to atrophy of individual muscle fibers rather than a reduction in the number of muscle fibres, and that muscle fibers in the masseter muscle may be more resistant to atrophy associated with ALS-like symptoms.

With regard to muscle fibre types, slow-twitch fibres are primarily MyHC-I, whereas fast-twitch fibres are mainly MyHC-IIa, IIb, and IIx, with a higher proportion of IIa fibers in humans and IIb fibers in mice[40,41]. Notably, MyHC-IIb fibres have strong fast-twitch properties, whereas MyHC-IIa fibres are intermediate and share characteristics with slow-twitch fibres. Our study found that both the masseter and gastrocnemius muscles were rich in fast-twitch MyHC-IIa and MyHC-IIb fibres, consistent with previous reports[42,43]. In mSOD1, the gastrocnemius muscle showed a decrease in the proportion of MyHC-IIb fibres in the late stage; however, the masseter muscle did not exhibit any such change in fibre type proportions. Previous research using this model has indicated that muscle weakness in the early stages typically occurs in glycolytic fibres, with a shift from glycolytic to oxidative fibre types as the disease progresses[44]. This is due to the loss of the fast fatigable motor unit composed of motoneurons innervating fast glycolytic fibres, and it has been thought that muscle atrophy occurs due to the destruction of the neuromuscular junction[39]. The stable fibre type proportion in the masseter muscle in our study suggests that it may be less susceptible to muscle fibre atrophy.

Muscle repair requires protein production and an increase in myofibre nuclei[19,20], and satellite cells (SCs), stem cells within skeletal muscle, are considered crucial to this process because they are required to supply myofibre nuclei[21–25,45]. Regarding the number of myonuclei per muscle fibre, the number of myonuclei was decreased in the gastrocnemius muscle of late-stage mSOD1, but was maintained in the masseter muscle. Furthermore, in the masseter muscle of end-stage mSOD1, the number of Pax7-positive SCs increased, but MyoD-positive SCs were unchanged. This suggests that the masseter muscle of mSOD1 contains a large pool of SCs from the quiescent to early active phase, but no increase in SCs after the active phase. Extraocular muscles

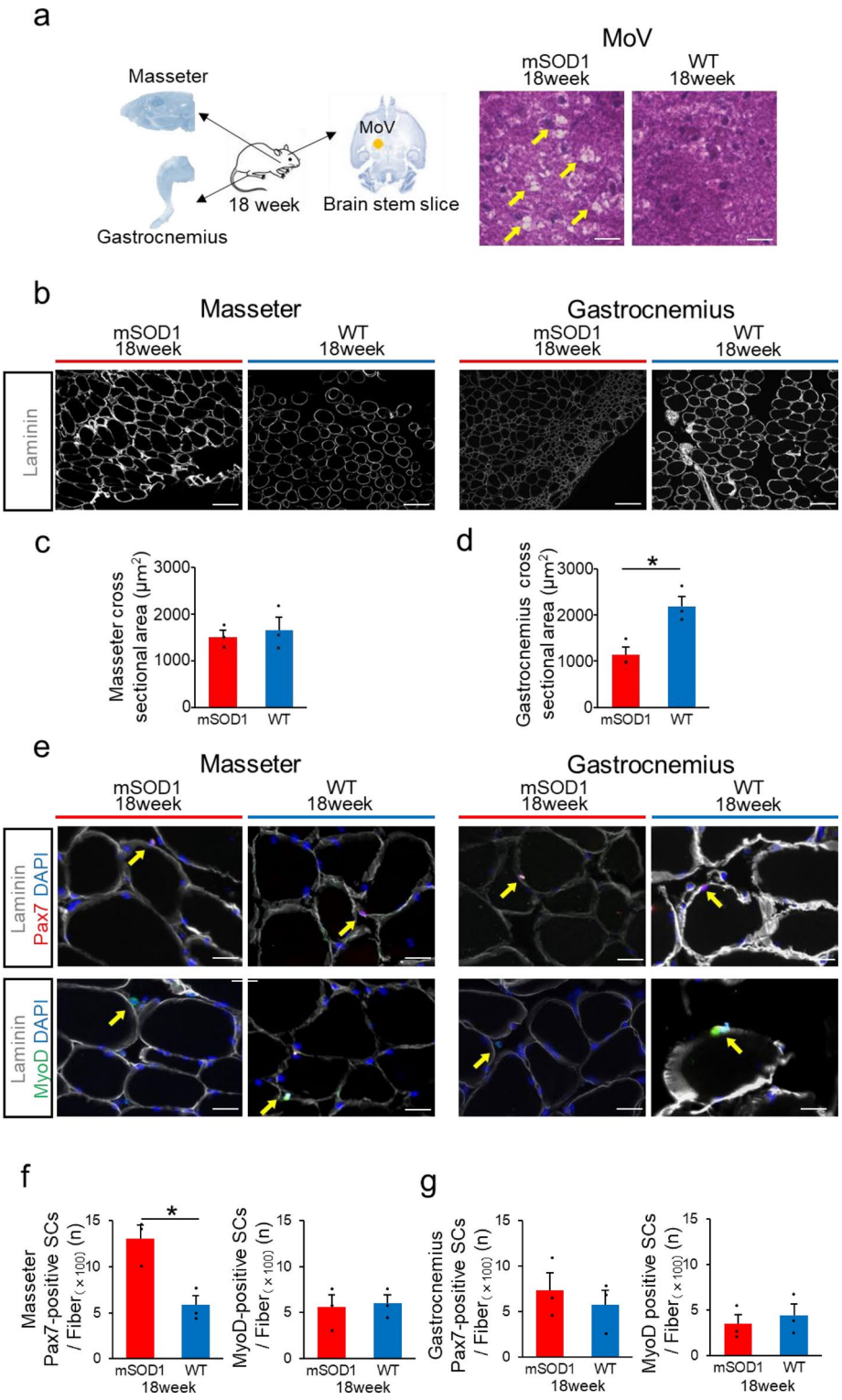

have also been reported to have a high number of SCs in patients with ALS[46,47]. In addition, compared to muscles such as the gastrocnemius, soleus, and diaphragm, the masseter muscle in mice has a higher number of SCs, suggesting a greater regenerative capacity[48]. Given the known relationship between myonuclear mass and muscle volume[49–51], an increase in the number of SCs in the masseter muscle of mSOD1 could be the key to maintaining the number of myonuclei and thus the muscle volume.

However, the exact role of SCs is not fully understood because ALS is usually a disease that does not involve direct muscle injury. In most cases, SCs are activated and proliferate within muscle fibers under conditions of overload, regardless of the degree of degeneration or injury[52] .This suggests that the progression of ALS-like symptoms may be overloading skeletal muscle. Previous studies have highlighted problems with myotube formation and functional abnormalities similar to age-related changes in SCs extracted from patients with ALS, and similar observations have been made in mSOD1[36,48,49]. Unlike the gastrocnemius muscle, the mechanism

◀**Fig. 7**. Analysis of Pax7 and MyoD expression in end-stage of mSOD1 (**a**) The brain stem, masseter muscle, and gastrocnemius muscle were extracted from mice that survived up to 18 weeks. Brain stem slices containing trigeminal motor nuclei (MoV) were prepared from the brain stem and performed H&E staining. The mSOD1 group mice showed vacuolation around MoV. (**b**) Fluorescent immunostaining showing Laminin (in gray) in the masseter and gastrocnemius muscles for both mSOD1 and WT groups at 18 weeks (scale bar: 100 μm). (**c**) Analysis of the cross-sectional area of muscle fibers in the masseter muscle for 18 weeks revealed no significant differences. (**d**) Cross-sectional area of muscle fibers in the gastrocnemius muscle at 18 weeks, indicating significantly smaller areas in the mSOD1 group [(mSOD1: n = 3, WT: n = 3), assessed using student's t-test, $p = 0.021$, $^{*}p < 0.05$]. (**e**) Fluorescent immunostaining displaying Laminin (in gray), DAPI (in blue), Pax7 (in red), and MyoD (in green) in the masseter and gastrocnemius muscles of the mSOD1 and WT group at 18 weeks (scale bar: 20 μm). Arrows point to satellite cells. Pax7-positive satellite cells are pink and MyoD-positive satellite cells are turquoise. (**f**) Pax7-positive satellite cells count per 100 muscle fibers in the masseter muscle were significantly increased in the mSOD1 group compared to the WT grou at 18 weeks, but MyoD-positive satellite cells showed no increase. [Pax7 (mSOD1: n = 3, WT: n = 3), assessed using student 's t-test, $p = 0.014$, $^{*}p < 0.05$, MyoD (mSOD1: n = 3, WT: n = 3)]. (**g**) Pax7-positive satellite cells count per 100 muscle fibers in gastrocnemius muscles were not significantly increased in the mSOD1 group compared to the WT group at 18 weeks, and MyoD-positive satellite cells showed no increase [Pax7 (mSOD1: n = 3, WT: n = 3), MyoD (mSOD1: n = 3, WT: n = 3)].

by which Pax7-positive SCs in the masseter muscle were increased and the masseter muscle volume was not atrophied requires further study.

The question of where ALS begins remains controversial among many researchers. In contrast to the theory that it begins at the neuromuscular junction, the 'dying back' theory states that muscle initiates a series of pathological events that promote the distal onset of motor neuron degeneration[13,14]. The metabolic properties of glycolytic fibres not only cause degradation of the neuromuscular junction, leading to characteristic symptoms of ALS, such as motor neuron death, but also metabolic changes in skeletal muscle may contribute to premature destabilization of the neuromuscular junction in ALS[39]. Understanding why skeletal muscle shows differential atrophy in ALS may pave the way for new therapeutic strategies for ALS that target peripheral tissues such as skeletal muscle.

Conclusion

In this study, we performed a comprehensive examination of feeding function and masseter muscle volume, alongside a histological analysis of the masseter and limb skeletal muscles in mSOD1. We observed that, despite a declined in limb motor functions, feeding function in these mice was preserved until the late stages of the disease. Remarkably, the masseter muscle did not show any reduction in muscle volume, wet weight, or cross-sectional area of muscle fibres. Furthermore, no changes were observed in muscle fibre types, indicating a possible resistance of the masseter muscle to ALS-induced impairment. A potential reason for the absence of atrophy in the masseter muscle could be its higher SC count compared with that in the gastrocnemius muscle. This abundance may support the maintenance of muscle fibre nuclei, aiding in muscle tissue regeneration. Further investigations into the different mechanisms of muscle atrophy could deepen our understanding of ALS pathology and aid in the development of therapeutic interventions.

Methods

Ethics statement

All animal experiments in this study were performed following the "Guidelines for Proper Conduct of Animal Experiments, 2006," as established by the Science Council of Japan. The study was approved by the Osaka University Recombinant DNA Experiment Safety Committee (Approval Number: 04538) and the Osaka University Graduate School of Dentistry Animal Experimentation Committee (Approval Number: D-HR-03-010-0).

Animals

We used male ALS model mice (JAX strain: C57B6SJL-Tg (SOD1G93A)1Gur/J) (mSOD1) and female wild-type mice (C57BL/6JJmsSlc) (WT) obtained from the Jackson Laboratory (Bar Harbor, MA, USA) for breeding purposes. For behavioural and physiological tests, including measurements of skeletal muscle volume, we used mice aged 4–16 weeks (male, mSOD1: n = 11, WT: n = 10). For fluorescence immunostaining and histological analysis, we used mice aged 8, 16 and 18 weeks (male, 8-week-old mSOD1: n = 5; 8-week-old WT: n = 5; 16-week-old mSOD1: n = 5; 16-week-old WT: n = 5; 18-week-old mSOD1: n = 3; 18-week-old WT: n = 3) (Table 1). The mice were individually housed in cages maintained at 23 °C with 60% humidity under a 12-h light/dark cycle, and had free access to solid feed (MF: Oriental Yeast, Tokyo, Japan)[6]. The ALS model mice in our study typically showed limb spasms and tremors at approximately 13 weeks and reached the end stage by approximately 20 weeks[53]. In behavioural and physiological studies, we monitored weight, muscle volume, eating ability, and motor function biweekly from 4 to 16 weeks of age. Mice older than 16 weeks were humanely euthanised immediately once they were unable to stand up on their own within 30 s of being placed on their sides[31]. All methods were performed in accordance with the relevant guidelines and regulations, as well as in accordance with the ARRIVE guidelines.

	WT	mSOD1
mouse	C57BL/6JJmsSlc	B6SJL-Tg (SOD1G93A)1Gur/J
Behavioral physiological Experiments	10	11
Immunofluorescence	13	13

Table 1. Number of mice used in each experiment.

Genotyping

For all analyses, 5 mm tail sections were collected from each mouse after the experiment to blind genotyping. DNA was extracted and purified from tail samples using the Quick-DNA Miniprep Plus Kit (ZYMO RESEARCH, Irvine, CA, USA). The genotyping was conducted via polymerase chain reaction (PCR), following the standard PCR protocol provided by The Jackson Laboratory [Protocol 29082: Standard PCR Assay – Tg (SOD1)][32].

Measurement of feeding function and body weight

For assessing Feeding function, the measured parameters included "Body weight," "Feeding time," and "Feeding volume," in line with previous studies[6]. The mice underwent a 12-h fasting period before observing their eating behaviour. The solid feed was secured to the side of the breeding cage, and the eating behaviour was recorded for 30 min using two video cameras (HANDYCAM, model HDR-XR520V: Sony Corporation, Tokyo, Japan; Everio, model GZ-HM890: Victor Company of Japan, Kanagawa, Japan) from two side angles (115 mm and 165 mm away from the feed). The "Feeding time" was defined as the total duration of eating within the observation period, and the "Feeding volume" was determined by the change in feed mass from the beginning to the end of the observation period[6]. Body weight was measured concurrently with muscle volume.

Measurement of limb motor function

Limb motor function was measured by focusing on running ability and grip strength. For determining running ability, we used a multilane treadmill (TMS-8N system; MELQUEST, Toyama, Japan) following the protocol reported by Reynolds et al.[54]. To prepare the mice, we conducted a 20-min training run at 13 m/min for three days before the actual measurement. The test comprised four stages, with a potential duration of up to 60 min. Initially, the mice ran at 13 m/min for 5 min. The speed was gradually increased to 18 m/min over the next 5 min. The third stage involved running at a constant of 18 m/min for 30 min. Finally, the speed was increased to 23 m/min, and the mice ran for an additional 20 min. The total distance for a complete 60-min run was 1142.5 m. To encourage running, the treadmill's rear had a grid with a mild electric current, which was harmless to the mice. If a mouse climbed onto the grid, it was gently encouraged to reengage with the treadmill using a paint brush, a long tool with a soft end. Mice that remained on the grid for 30 s were considered fatigued, and their running distances were recorded at that point. The grip strength was assessed using a grip strength meter (GPM-101BV; MELQUEST, Toyama, Japan)[54]. Measurements were taken six times per day, with a minimum one-min rest between each attempt, avoiding running ability test or fasting days. The process was repeated the following day, and the average value was recorded as the final measurement value[55].

Measurement of masseter and limb muscle volumes in mice

To measure the volumes of the masseter and limb muscles, mice were initially sedated using an intraperitoneal injection comprising medetomidine hydrochloride (0.02 mg/kg), midazolam (0.3 mg/kg), and butorphanol tartrate (0.2 mg/kg), followed by weighing. To ensure consistent imaging postures, the participants were positioned on a specifically designed imaging stand. Separate imaging of the head, forearms, and hind limbs was conducted using a micro-CT scanner (R_mCT2: Rigaku Corporation, Tokyo, Japan), with the settings adjusted to a tube voltage of 90 kV, a current of 160 μA, and a voxel resolution of 148 μm^3, foregoing the use of contrast agents. The obtained images were processed using TRI/3D-BONE software (RATOC, Tokyo, Japan) to delineate and quantify the masseter and limb muscle volumes. For masseter muscle analysis, the skull orientation was adjusted so as to align the palatine bone of the mouse horizontally with the ground in sagittal views and the nasal septum vertically in coronal views. The masseter muscle boundaries were delineated in frontal views, visually identifying the origin and termination points. To define the cross-sectional area, a mask was applied to the region encompassing the masseter muscle, excluding the jawbone and air space. The methodology for outlining the masseter muscle morphology on CT scans was adapted from a study by Jeffery et al.[56,57]. The masseter muscle volume was calculated from the front to the back edge of the mandibular ramus. Limb muscles were analysed separately for the fore and hind limbs. Forelimb analysis primarily targeted the triceps brachii, mapping it from the elbow to the head of the ulna in the coronal view. Hindlimb analysis focused on the gastrocnemius muscle, delineated in frontal views from the knee to the tarsocrural joint[37]. The cumulative volumes of these muscle groups represent the total limb muscle volume. A skilled individual performed all volume measurements.

Measurement of masseter and gastrocnemius muscle weight and preparation of frozen samples

For this part of the study, we used male mSOD1 and WT aged 8, 16 and 18 week. The mice were euthanised by cervical dislocation, and their masseter and gastrocnemius muscles were promptly removed, ensuring that no excess tissue was included. We measured muscle weights, which included their water content. After excision, muscle tissues were immediately frozen in 2-methylbutane and cooled with liquid nitrogen. The tissues were

	Dilution	Supplier	Antibody Registry ID
laminin α2 (clone 4H8-2)	1:500	Enzo Life Sciences	AB_2051764
PAX7 Antibody (PA1-117)	1:200	Thermo Fisher	AB_2539886
BA-D5 (MyHC-I)	1:200	Developmental Studies Hybridoma Bank	AB_2235587
SC-71 (MyHC-IIa)	1:300	Developmental Studies Hybridoma Bank	AB_2147165
BF-F3 (MyHC-IIb)	1:200	Developmental Studies Hybridoma Bank	AB_2266724
Alexa Flaor 647 chicken anti Rat IgG(H + L)	1:1000	Thermo Fisher	AB_2535875
Alexa Flaor Plus 555 Goat anti Rabbit IgG (H + L)	1:1000	Thermo Fisher	AB_2633281
Alexa Flaor 546 goat anti Mouse IgG2b	1:1000	Thermo Fisher	AB_2535779
Alexa Flaor 546 goat anti Mouse IgM	1:1000	Thermo Fisher	AB_2535714
Alexa Flaor 546 goat anti Mouse IgG1	1:1000	Thermo Fisher	AB_2535765

Table 2. Antibodies and dilution concentrations.

then placed on dry ice for 1 h to allow 2-methylbutane to evaporate before storing them in sealed containers at− 80 °C[58]. To prevent drying, the muscle tissue was moistened using phosphate-buffered saline (PBS) from the time of euthanasia until freezing.

Fluorescence imaging and microscopy

For this procedure, frozen tissue samples were cut into 6-µm-thick sections using a cryostat and placed on slide glasses. They were dried at temperatures between 15 ℃ and 25 ℃ for 30 min. A PAP pen was used to outline the periphery of each section to prevent leakage of the solution. The sections were fixed in 4% paraformaldehyde for 10 min, followed by two 5-min washes with 0.1% Triton X-100/PBS (PBST) and a 5-min rinse in PBS. The slides were placed in a humidity chamber and blocked with 5% skim milk/PBS at 37 ℃ for 1 h. For Pax7 and MyoD staining, after paraformaldehyde fixation, the sections were treated with 0.5% PBST for 20 min, and washed twice with PBST and once with PBS for 5 min each. The primary antibodies were diluted in 5% skim milk/PBS and left to incubate overnight at 4 ℃. The following day, the sections were washed twice with PBST and once with PBS, for 5 min each time, and were incubated for 1 h at room temperature with secondary antibody dilutions. This was followed by two more PBST washes and one PBS wash, each lasting for 5 min, before mounting with a DAPI-containing medium[58]. All images of the fluorescent immunostained sections were obtained using an all-in-one fluorescence microscope (BZ-X800, KEYENCE, Osaka, Japan) with a Plan Apochromat 20 × objective (NA0.75, BZ-PA20, KEYENCE, Osaka, Japan). All the specimens were processed by the same experienced technician. The antibodies used for fluorescence immunostaining are listed in Table 2.

Quantitative analysis of muscle fibres in masseter and gastrocnemius muscles

Each fluorescence signal was automatically calculated using a hybrid cell count application (BZ-H4C, KEYENCE, Osaka, Japan) using the BZ-X Analyser software (BZ-H4A, KEYENCE, Osaka, Japan). Initially, we adjusted the threshold to identify the fluorescent signals of laminin-positive basement membranes. The separation function of the software was employed to isolate individual muscle fibres. The lower limit of the histogram function was adjusted to avoid including erroneously identified small areas[59,60]. Subsequently, the number of muscle fibres and their cross-sectional areas were automatically calculated for each sample. In total, we analysed 1370.9 ± 144.12 fibres in the masseter and 2252.35 ± 210.51 fibres in the gastrocnemius, across 20 samples from all age groups. The muscle fibre types were classified by staining consecutive sections for MyHC-I, MyHC-IIa, and MyHC-IIb, with the fluorescence signal for each type identified and quantified separately[44]. The nuclei were counted with the help of laminin/DAPI-positive signals. We found an average of 3.94 ± 0.28 nuclei per fibre in the masseter and 2.64 ± 0.31 nuclei per fibre in the gastrocnemius from the same 20 samples. SC quantities were assessed with the help of Pax7/DAPI-positive and Myod/DAPI-positive signals. Pax7/DAPI-positive SCs indicated 9.24 ± 1.20 SCs per 100 fibres in the masseter and 4.31 ± 0.67 SCs per 100 fibres in the gastrocnemius.

Quantification and statistical analysis

Statistical analyses were conducted using IBM SPSS Statistics software (IBM, Chicago, IL, USA). To assess data normality, we performed the Kolmogorov–Smirnov or Shapiro–Wilk tests, and evaluated variance homogeneity via Levene's test. The Student's t-test was used to analyse independent subsets. All data are presented as mean ± standard error. We compared parameters such as body weight, muscle volume, feeding time, food intake, running distance, and grip strength between the WT and mSOD1 groups via two-way repeated measures ANOVA. In cases where an interaction between groups was observed, post-hoc comparisons were conducted using the Tukey–Kramer test. The threshold for statistical significance was set at 5%.

Data availability

Raw data were generated at Department of Oral and Maxillofacial Surgery, Graduate School of Dentistry, Osaka University. Derived data supporting the findings of this study are available from the corresponding author S.S on request.

Received: 18 March 2024; Accepted: 27 September 2024
Published online: 16 October 2024

References

1. Kiernan, M. C. *et al.* Amyotrophic lateral sclerosis. *Lancet* **377**, 942–955 (2011).
2. Shimizu, T. *et al.* Prognostic significance of body weight variation after diagnosis in ALS: A single-centre prospective cohort study. *J. Neurol.* **266**, 1412–1420 (2019).
3. Perry, B. J., Nelson, J., Wong, J. B., Kent, D. M., Pooled Resource Open-Access ALS Clinical Trials Consortium. Predicting dysphagia onset in patients with ALS: The ALS dysphagia risk score. *Amyotroph. Lateral Scler. Frontotemporal Degener.* **23**, 271–278 (2022).
4. Robison, R. *et al.* Swallowing safety and efficiency impairment profiles in individuals with amyotrophic lateral sclerosis. *Dysphagia* **37**, 644–654 (2022).
5. Petrov, D., Mansfield, C., Moussy, A. & Hermine, O. ALS clinical trials review: 20 years of failure. Are we any closer to registering a new treatment?. *Front. Aging Neurosci.* **9**, 68 (2017).
6. Kitaoka, Y. *et al.* Analysis of feeding behavior characteristics in the Cu/Zn. Superoxide dismutase 1 (SOD1) SOD1G93A mice model for amyotrophic lateral sclerosis (ALS). *Nutrients* **15**, 1651 (2023).
7. Seki, S. *et al.* Characteristics of sensory neuron dysfunction in amyotrophic lateral sclerosis (ALS): Potential for ALS therapy. *Biomedicines* **11**, 2967 (2023).
8. Tanaka, S., Seki, S., Ono, Y., Enomoto, A. & Kogo, M. Persistent sodium conductance contributes to orexin-A-mediated modulation of membrane excitability in neonatal rat mesencephalic V neurons. *Neurosci. Lett.* **753**, 135846 (2021).
9. Seki, S. *et al.* Neuropeptide Y modulates membrane excitability in neonatal rat mesencephalic V neurons. *J. Neurosci. Res.* **98**, 921–935 (2020).
10. Seki, S. *et al.* Circuit-specific early impairment of proprioceptive sensory neurons in the SOD1(G93A) mouse model for ALS. *J. Neurosci.* **39**, 8798–8815 (2019).
11. Venugopal, S., Hsiao, C. F., Sonoda, T., Wiedau-Pazos, M. & Chandler, S. H. Homeostatic dysregulation in membrane properties of masticatory motoneurons compared with oculomotor neurons in a mouse model for amyotrophic lateral sclerosis. *J. Neurosci.* **35**, 707–720 (2015).
12. Pun, S., Santos, A. F., Saxena, S., Xu, L. & Caroni, P. Selective vulnerability and pruning of phasic motoneuron axons in motoneuron disease alleviated by CNTF. *Nat. Neurosci.* **9**, 408–419. https://doi.org/10.1038/nn1653 (2006).
13. Ragagnin, A. M. G., Shadfar, S., Vidal, M., Jamali, M. S. & Atkin, J. D. Motor neuron susceptibility in ALS/FTD. *Front. Neurosci.* **13**, 532. https://doi.org/10.3389/fnins.2019.00532 (2019).
14. Bette, M., Cors, E., Kresse, C. & Schütz, B. Therapeutic treatment of superoxide dismutase 1 (G93A) amyotrophic lateral sclerosis model mice with medical ozone decelerates trigeminal motor neuron degeneration, attenuates microglial proliferation, and preserves monocyte levels in mesenteric lymph nodes. *Int. J. Mol. Sci.* **23**, 3403. https://doi.org/10.3390/ijms23063403 (2022).
15. Venugopal, S. *et al.* Early deficits in GABA inhibition parallels an increase in L-type Ca2+ currents in the jaw motor neurons of SOD1G93A mouse model for ALS. *Neurobiol. Dis.* **177**, 105992. https://doi.org/10.1016/j.nbd.2023.105992 (2023).
16. Hwang, C. S., Weng, H. H., Wang, L. F., Tsai, C. H. & Chang, H. T. An eye-tracking assistive device improves the quality of life for ALS patients and reduces the caregivers' burden. *J. Mot. Behav.* **46**, 233–238 (2014).
17. Pikatza-Menoio, O., Elicegui, A. & Bengoetxea, X. The skeletal muscle emerges as a new disease target in amyotrophic lateral sclerosis. *J. Pers. Med.* **11**, 671 (2021).
18. Nijssen, J., Comley, L. H. & Hedlund, E. Motor neuron vulnerability and resistance in amyotrophic lateral sclerosis. *Acta Neuropathol.* **133**, 863–885. https://doi.org/10.1007/s00401-017-1708-8 (2017).
19. Schiaffino, S., Dyar, K. A., Ciciliot, S., Blaauw, B. & Sandri, M. Mechanisms regulating skeletal muscle growth and atrophy. *FEBS J.* **280**, 4294–4314 (2013).
20. Dumont, N. A., Bentzinger, C. F., Sincennes, M. C. & Rudnicki, M. A. Satellite cells and skeletal muscle regeneration. *Compr. Physiol.* **5**, 1027–1059 (2015).
21. Egner, I. M., Bruusgaard, J. C. & Gundersen, K. Satellite cell depletion prevents fiber hypertrophy in skeletal muscle. *Development* **143**, 2898–2906 (2016).
22. Fry, C. S. *et al.* Regulation of the muscle fiber microenvironment by activated satellite cells during hypertrophy. *FASEB J.* **28**, 1654–1665 (2014).
23. Fukada, S. *et al.* Isolation, characterization, and molecular regulation of muscle stem cells. *Front. Physiol.* **4**, 317 (2013).
24. Sambasivan, R. *et al.* Pax7-expressing satellite cells are indispensable for adult skeletal muscle regeneration. *Development* **17**, 3647–3656 (2011).
25. Lepper, C., Partridge, T. A. & Fan, C. An absolute requirement for Pax7-positive satellite cells in acute injury-induced skeletal muscle regeneration. *Development.* **17**, 3639–3646 (2011).
26. Seale, P. *et al.* Pax7 is required for the specification of myogenic satellite cells. *Cell* **6**, 777–786 (2000).
27. Saltin, B., Henriksson, J., Nygaard, E., Andersen, P. & Jansson, E. Fiber types and metabolic potentials of skeletal muscles in sedentary man and endurance runners. *Ann. N. Y. Acad. Sci.* **301**, 3–29 (1977).
28. Peggion, C. *et al.* Absolute quantification of myosin heavy chain isoforms by selected reaction monitoring can underscore skeletal muscle changes in a mouse model of amyotrophic lateral sclerosis. *Anal. Bioanal. Chem.* **409**, 2143–2153. https://doi.org/10.1007/s00216-016-0160-2 (2017).
29. Scaricamazza, S. *et al.* Skeletal-muscle metabolic reprogramming in als-sod1g93a mice predates disease onset and is a promising therapeutic target. *iScience.* **23**, 101087. https://doi.org/10.1016/j.isci.2020.101087 (2020).
30. Pasetto, L. *et al.* Micro-computed tomography for non-invasive evaluation of muscle atrophy in mouse models of disease. *PLoS One.* **13**, e0198089. https://doi.org/10.1371/journal.pone.0198089 (2018).
31. Azzouz, M. *et al.* Progressive motor neuron impairment in an animal model of familial amyotrophic lateral sclerosis. *Muscle Nerve* **20**, 4551 (1997).
32. Oliván, S. *et al.* Comparative study of behavioural tests in the SOD1G93A mouse model of amyotrophic lateral sclerosis. *Exp. Anim.* **64**, 147–153 (2015).
33. Tankersley, C. G., Haenggeli, C. & Rothstein, J. D. Respiratory impairment in a mouse model of amyotrophic lateral sclerosis. *J. Appl. Physiol.* **1985**(102), 926–932 (2007).
34. Ruoppolo, G. *et al.* Dysphagia in amyotrophic lateral sclerosis: Prevalence and clinical findings. *Acta Neurol. Scand.* **128**, 397–401 (2013).
35. Kanning, K. C., Kaplan, A. & Henderson, C. E. Motor neuron diversity in development and disease. *Annu. Rev. Neurosci.* **33**, 409–440. https://doi.org/10.1146/annurev.neuro.051508.135722 (2010).
36. Manzano, R. *et al.* Altered in vitro proliferation of mouse SOD1-G93A skeletal muscle satellite cells. *Neurodegener. Dis.* **11**, 153–164 (2013).
37. Marcuzzo, S. *et al.* Hind limb muscle atrophy precedes cerebral neuronal degeneration in G93A-SOD1 mouse model of amyotrophic lateral sclerosis: A longitudinal MRI study. *Exp. Neurol.* **231**, 30–37 (2011).
38. Hwee, D. T. *et al.* Fast skeletal muscle troponin activator tirasemtiv increases muscle function and performance in the B6SJL-SOD1G93A ALS mouse model. *PLoS One* **9**, e96921 (2014).

39. Palamiuc, L. *et al.* A metabolic switch toward lipid use in glycolytic muscle is an early pathologic event in a mouse model of amyotrophic lateral sclerosis. *EMBO Mol. Med.* **7**, 526–546 (2015).
40. Murgia, M. *et al.* Protein profile of fiber types in human skeletal muscle: A single-fiber proteomics study. *Skelet Muscle.* https://doi.org/10.1186/s13395-021-00279-0 (2021).
41. Harrison, B. C. *et al.* Skeletal muscle adaptations to microgravity exposure in the mouse. *J. Appl. Physiol.* **95**, 2462–7240. https://doi.org/10.1152/japplphysiol.00603.2003 (2003).
42. Villalón, E., Lee, N. N., Marquez, J. & Lorson, C. L. Muscle fiber-type selective propensity to pathology in the nmd mouse model of SMARD1. *Biochem. Biophys. Res. Commun.* **516**, 313–319 (2019).
43. Widmer, C. G., Morris-Wiman, J. A. & Nekula, C. Spatial distribution of myosin heavy-chain isoforms in mouse masseter. *J. Dent. Res.* **81**, 33–38 (2002).
44. Hegedus, J., Putman, C. T., Tyreman, N. & Gordon, T. Preferential motor unit loss in the SOD1 G93A transgenic mouse model of amyotrophic lateral sclerosis. *J. Physiol.* **586**, 3337–3351 (2008).
45. McCarthy, J. J. *et al.* Effective fiber hypertrophy in satellite cell-depleted skeletal muscle. *Development* **138**, 3657–3666 (2011).
46. Ciciliot, S., Rossi, A. C., Dyar, K. A., Blaauw, B. & Schiaffino, S. Muscle type and fiber type specificity in muscle wasting. *Int. J. Biochem. Cell Biol.* **45**, 2191–2199 (2013).
47. Kallestad, K. M. *et al.* Sparing of extraocular muscle in aging and muscular dystrophies: A myogenic precursor cell hypothesis. *Exp. Cell Res.* **317**, 873–885 (2011).
48. Yamane, A., Akutsu, S., Diekwisch, T. G. & Matsuda, R. Satellite cells and utrophin are not directly correlated with the degree of skeletal muscle damage in mdx mice. *Am. J. Physiol. Cell Physiol.* **289**, C42–C48 (2005).
49. Hansson, K. A. *et al.* Myonuclear content regulates cell size with similar scaling properties in mice and humans. *Nat. Commun.* **11**, 6288 (2020).
50. Cramer, A. A. W. *et al.* Nuclear numbers in syncytial muscle fibers promote size but limit the development of larger myonuclear domains. *Nat. Commun.* **11**, 6287 (2020).
51. Ma, K. Reduced masticatory function is related to lower satellite cell numbers in masseter muscle. *Eur. J. Orthod.* **36**, 262 (2014).
52. Fukada, S. I., Akimoto, T. & Sotiropoulos, A. Role of damage and management in muscle hypertrophy: Different behaviors of muscle stem cells in regeneration and hypertrophy. *Biochim. Biophys. Acta Mol. Cell Res.* **1867**, 118742 (2020).
53. De Giorgio, F., Maduro, C., Fisher, E. M. C. & Acevedo-Arozena, A. Transgenic and physiological mouse models give insights into different aspects of amyotrophic lateral sclerosis. *Dis. Model. Mech.* **12**, dmm037424 (2019).
54. Reynolds, J. C. & Lee, C. Mouse fitness as determined through treadmill running and walking. *Methods Mol. Biol.* **2144**, 57–65 (2020).
55. Takeshita, H. *et al.* Modified forelimb grip strength test detects aging-associated physiological decline in skeletal muscle function in male mice. *Sci. Rep.* **7**, 42323 (2017).
56. Jeffery, N. & Mendias, C. Endocranial and masticatory muscle volumes in myostatin-deficient mice. *R. Soc. Open Sci.* **1**, 140187 (2014).
57. Pasetto, L. *et al.* Micro-computed tomography for non-invasive evaluation of muscle atrophy in mouse models of disease. *PLoS One* **13**, e0198089 (2018).
58. Kaneshige, A. *et al.* Detection of muscle stem cell-derived myonuclei in murine overloaded muscles. *Star Protoc.* **3**, 101307 (2022).
59. Uezumi, A. *et al.* Mesenchymal Bmp3b expression maintains skeletal muscle integrity and decreases in age-related sarcopenia. *J. Clin. Invest.* **131**, e139617 (2021).
60. Ozawa, T., Miyazono, K. & Morikawa, M. Preparation of monovalent follistatin-like 3-Fc-fusion protein and evaluation of its effects on muscle mass in mice. *Star Protoc.* **2**, 100839 (2021).

Acknowledgements

This study was supported by the Center for Medical Research and Education of the Graduate School of Medicine, Osaka University, Japan.

We extend our deepest gratitude to Dr. Yutaka Matsushita for providing invaluable insights into the measurement of muscle volume in mice. His expertise has greatly enhanced the quality of our research.

Author contributions

Conceptualization, S.S.; methodology, Y.K., K.K. and S.S.; validation, S.K., S.S., A.N., Y.K., K.I., S.-i.F., M.K. and S.T.; investigation, S.K. and S.S.; data collection, S.K., writing original draft preparation, S.K. and S.S.; wright review and editing, S.S.; supervision., S.S. and S.T.; project administration, S.S. and S.T.; funding acquisition, S.S. and M.K. All authors have read and agreed to the published version of the manuscript.

Funding

This research was funded by JSPS KAKENHI (grant numbers: 19K24117, 21K17088, 20H03887).

Competing interests

The authors declare no Competing Interests.

Additional information

Correspondence and requests for materials should be addressed to S.S.

Reprints and permissions information is available at www.nature.com/reprints.

Publisher's note Springer Nature remains neutral with regard to jurisdictional claims in published maps and institutional affiliations.